A NOVEL TRIPLE-BAND ELECTROMAGNETIC BANDGAP (EBG) STRUCTURE

Huynh Nguyen Bao Phuong[1] , Dao Ngoc Chien[2] and Tran Minh Tuan[3]
[1]Hanoi University of Science and Technology, Hanoi, Vietnam
[2]Ministry of Science and Technology, Hanoi, Vietnam
[3]Ministry of Information and Communications of Vietnam, Hanoi, Vietnam

ABSTRACT

A novel triple-band uni-planar electromagnetic bandgap (UC-EBG) structure is proposed in this paper. This EBG structure can be considered as distorted uni-planar compact-EBG (DUC-EBG) which is connected together by the meandered line inductor. Split ring resonators (SRR) are embedded in four pad corners and two L-shaped slots are etched at the central pad. The proposed EBG structure is modelled in three equivalent circuits. By using in-house developed computational code based on the FDTD method, simulated results of dispersion diagrams are presented by complete triple-bandgap. The central frequency of the bandgaps can be reduced to the lower region without increasing the size of the EBG cell. Moreover, an array of 4×5 EBG cells was simulated, fabricated and measured to verify the bandgap characteristic through the transmission coefficient S21. This proposed EBG can be used for multi-band applications, such as dual/triple antennas.

KEYWORDS: *Electromagnetic bandgap, Triple-band, and Dispersion Diagram*

I. INTRODUCTION

In recent years, high impedance surfaces (HIS) have attracted considerable attention to improve antenna's performance. High impedance surfaces have two main possible behaviors: artificial magnetic conductor (AMC) properties and electromagnetic bandgap (EBG) properties that lead to the surface wave suppression and in-phase reflection coefficient properties [1]-[4]. EBG structure is a periodical cell included of a metallic or dielectric element. The unique characteristic of EBG structures is to exhibit bandgap feature in the suppression of surface wave propagation. Many studies have been carried out in electromagnetic bandgap structures. Several EBG structures have been proposed for applications in the electromagnetic and antennas community. As typical uses, it has been integrated with antennas to enhance the gain and to reduce the backward radiation by suppressing surface wave, thus improving efficiency [3]. The bandgap characteristics depend on the material properties such as dimensions, periodicity and permittivity [5].

As early EBG lattice periods were half-wavelength at the center bandgap frequency, practical applications of EBG structures had difficulties in accommodating their physical sizes. This problem has not been solved until the mushroom-like EBG proposed by Sievenpiper et al. [6]. However, the mushroom EBG structure has large size when operating at low frequencies. The requirements of the EBG structures in most microwave applications are a small unit cell size. Moreover, it is necessary to design the EBG structures that could be introduced dual-bandgap or triple-bandgap for multi-band applications. In previously published papers, several dual-band EBG structures were proposed [7]-[9]. In [7] and [8], dual-band structures were achieved by using via but the fabrication is more complex. Besides, in [8], two EBG structures with different shape are used. A cascaded EBG of ten unit cells was proposed to introduce dual-bandgap [9]. In which, the vias are moved off the center of six patches and placed at the center of four rest ones. Therefore, two above EBG structure also enlarged the total size of the structure.

Besides, several triple-band EBG structures were also presented in the literature [10]-[12]. A triple-band EBG, which is using Sierpinski Gasket was proposed in [10]. In this design, the EBG was formed by combining four Sierpinski triangles at step 1 and step 2. However, two of four triangular patches are connected to the solid lower ground plane by a metal plated via, which is leading to more complexity in the fabrication. Similarly, in [11] an EBG structure was designed by combining a metal patch with the Mandelbrot Fractal at the 2nd iteration. As results, this EBG structure can produce triple-bandgap, but the limitation of this structure also uses metal via. Moreover, a novel compact EBG structure constructed by etching a complementary split ring resonator on the patch of a conventional mushroom-like EBG was proposed by Lin Peng et al [12]. This EBG structure introduced triple-bandgap, but only the first bandgap is defined in all directions in the surface structure. Another two bandgap in Y-direction are observed. It is a real challenging task to obtain a UC-EBG structure with complete triple-bandgap.

In this paper, the novel triple-band uni-planar EBG structure is proposed. This triple-band UC-EBG is simply a distorted conventional UC-EBG. As the result, the complete triple-bandgap allows to suppress the surface wave propagation in all directions. The remainder of this paper is organized as follows. In Section II, the detailed designs of the novel UC-EBG are presented. By using an in-house developed computational tool based on the finite-difference time domain (FDTD) method [13], the simulation of dispersion properties and transmission coefficient are shown in Section III. Besides, the measurement of the proposed EBG structure in fabrication is also utilized, while the conclusions are provided in Section IV.

II. DESIGN OF TRIPLE-BAND EBG STRUCTURE

The EBG structure actually forms an equivalent distributed *LC* circuit with specific resonant frequencies. The electromagnetic properties of the EBG structure can be described using its equivalent capacitors and equivalent inductors. In the bandgap frequency range, the surface impedance of an EBG structure is very high and EBG will be operating as a band-stop with some frequency ranges and the collecting of these resonant frequencies lead to forms the bandgap property of EBG. Therefore, it will block the flow of the surface waves. The bandgap frequency can be considered as the resonant frequency of the equivalent *LC* network. The central frequency of the bandgap is defined as follows [6]:

$$f_C = \frac{1}{2\pi\sqrt{LC}} \tag{1}$$

Here, f_C is estimated by the following equation:

$$f_C = \frac{f_{\max} + f_{\min}}{2} \tag{2}$$

Note that $f_{\max}$ and $f_{\min}$ are the maximum and the minimum frequency of the bandgap, respectively.

The conventional UC-EBG is shown in Fig. 1(a). The gaps between the conductor edges of two adjacent cells introduce equivalent capacitance *C*. In addition, the narrow strips, connected the two patches, introduce equivalent inductance L. Thus, it can be described using the equivalent *LC* circuit, as shown in Fig. 1(b).

From the UC-EBG structure above, it is observed that the only single bandgap was formed. In order to obtain a triple-band EBG structure, it is proposed to introduce three bandgaps separately. The first bangap is created similarly as the conventional UC-EBG. The second and the third ones are created by introducing more equivalent capacitance *C* and inductance *L*. These bandgaps can be obtained by etching some proper shape on the surface of the UC-EBG cell.

The schematic of the proposed triple-band UC-EBG structure is shown in Fig. 2. The proposed structure can be represented by three different equivalent circuits as shown in Fig. 3. The first bandgap is formed by meandered line and the gaps between the conductor edges of two adjacent cells. The meandered line introduces the equivalent inductance L_1, the gaps introduces the equivalent capacitance C_1. In this design, parasitic capacitances C_{Pi}, which are produced by the steps of the meandered lines, as shown in Fig. 3(a), will allow to increase the total capacitance of the equivalent

circuit, and hence move down the bandgap of the structure to a lower frequency region. Here, the lower bandgap can also be understood that the size of EBG can be reduced with the same electromagnetic bandgap. The equivalent circuit is described in Fig. 3(a). The frequency of the first bandgap can be determined as follows:

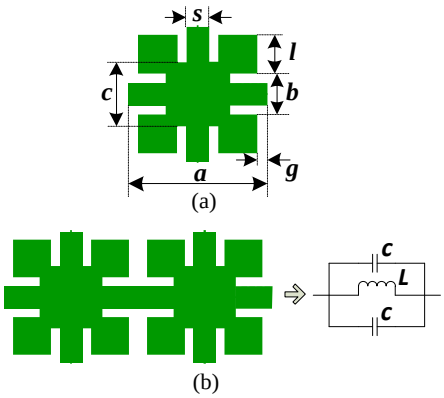

Figure 1: Conventional UC-EBG structure (a) Unit cell and (b) Equivalent circuit

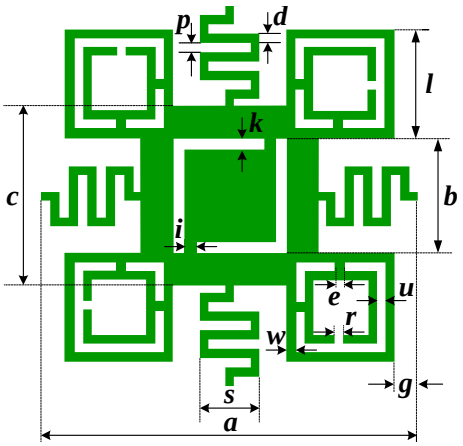

Figure 2: Novel triple-band UC-EBG

$$f_{C1} = \frac{1}{2\pi\sqrt{L_1\left[C_1 + \left(2\sum_{i=1}^{n}\frac{1}{C_{Pi}}\right)^{-1}\right]}} \tag{3}$$

Note that *n* denoted the number steps of the meandered line. In the proposed EBG structure, the value of *n* is 4.

When the SRRs are embedded in corner pads, the second bandgap can be obtained. The total capacitance with SRR consists of two parts. One part is the coupling capacitance C_C between the outer and the inner rings. The other one is produced the electric charges accumulate at the split.

In the Fig. 3(b), the equivalent capacitances C_{21} and C_{22} engendered by the voltage gradients between SRR gap (*u*). Moreover, the split of the inner ring with gap *r* is introduced the equivalent capacitance C_{23}. The current flowing along SRR coil (with width *w*) indicated by dash arrows produces the inductance L_2. The additional inductance can be obtained by two strips, which are connected between the outer and inner ring.

The coupling capacitance C_C can be estimated by the following equation [14]:

$$C_C = \left[0.06 + 3.5\times10^{-5}\left(r_{out} + r_{in}\right)\right] \tag{4}$$

Then the coupling capacitance should be divided into four equal counter parts named C_0 for SRR four sides [15], thus:

$$C_0 = \frac{1}{4}\left[0.06 + 3.5\times10^{-5}\left(r_{out} + r_{in}\right)\right] \tag{4a}$$

Here r_{out} and r_{in} represent the radius of the outer and the inner circumcircle of the SRR ring.

It is vital to estimate the capacitances at the inner split, but it is difficult because of the intense electromagnetic brink effects. So they are estimated as the following approaches:

$$C_{inner\ split} = 3\varepsilon_0 u / r \tag{4b}$$

Note that, ε_0 is the permittivity in a vacuum.

The equivalent capacitances of the SRR in the proposed EBG structure are estimated as follows:

$$C_{21} = 3C_0;\ C_{22} = C_0 \text{ and } C_{23} = C_{inner\ split} \tag{4c}$$

Thus, the central frequency of the second bandgap of the equivalent circuit shown in Fig. 3(b):

$$f_{C2} = \frac{1}{2\pi\sqrt{L_2\left(C_{23}+C_{21}+C_{22}\right)}} \tag{4d}$$

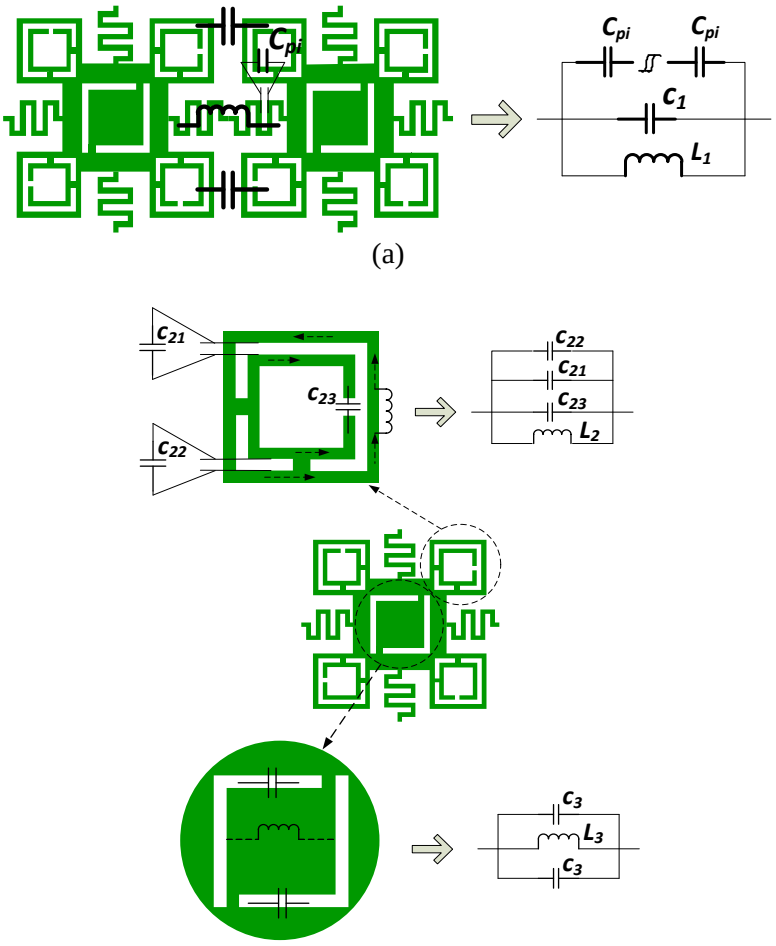

Figure 3: Equivalent circuits of the triple-band UC-EBG
(a) First bandgap and (b) Second and third bandgap

In order to create the symmetry of the proposed structure, the SRRs are embedded in four corner pads. The inner ring would be rotated in a clockwise without changing the second bandgap.
Finally, two L-shaped slots was etching symmetry in the center of the patch. The width *k* of slot introduced the equivalent capacitance C3 and the square pad that connects two slots can be result in equivalent inductance L_3. As the result it can be described by another equivalent circuit which is defined the third bandgap independently as the others bandgap.
However, there is another method to easily predict the third central frequency f_{C3} of the proposed EBG structure. This frequency is considered as the resonant frequency of a slot that is defined by the following formula:

$$f_{slot} = \frac{c}{4L_{slot}\sqrt{\varepsilon_{eff}}} \tag{5}$$

Here, *c* denoted the light velocity and ε_{eff} *is* the effective permittivity, which is expressed as [16]:

$$\varepsilon_{eff} = \frac{\varepsilon_r + 1}{2} \tag{5a}$$

The length of the L - shaped slot is defined as follows:

$$L_{slot} = 2b - (k + i) \tag{5b}$$

Here *b* is the length of the vertical edge of the slot and *i* is the space between the ends of two slot.

III. SIMULATION SETUP AND DISCUSSIONS

The simulation of the triple-band UC-EBG (TUE) and the conventional UC-EBG (CUE) is utilized. In order to take two structures into the comparison, the following parameters are the same: the substrate material is FR4 with the dielectric constant ε_r = 4.4 and substrate thickness h = 1.6. The periodic spacing are all chosen as a = 7.2 mm. The length of conductor edges is l = 2 mm and the gap between conductor edges of two adjacent cells is g = 0.6 mm. The design parameters for each of these structures are summarized in Table 1.

In general, the bandgap of EBG structure can be fully expressed by using dispersion diagrams. Besides, the features of bandgap also can be determined through the transmission coefficient S21. Thus, in order to verify the bandgap properties of the proposed structure, the both methods for investigating the proposed EBG structure are utilized in sequence. Firstly, the dispersion diagram is investigated to define the bandgaps. The bandgaps of EBG structure are evaluated from the dispersion analysis on only one cell and not on an array of EBG cells. An infinite structure is simulated by imposing periodic boundary conditions with appropriate phase shifts onto the unit cell in a suitable eigenmode solver. Wave propagation in the structure can be represented by certain vectors in a unit cell that constitutes a boundary region of propagation, often referred to as the irreducible Brillouin zone. Deriving the propagating modes in this zone allows covering all the possible directions of propagating within a unit cell.

Note that the dispersion analysis can only be utilized when the EBG is a periodic structure and central symmetry. Conversely, the bandgap will not be appearing in the dispersion diagram. The proposed EBG structure has successfully designed to satisfy two above conditions. Fig. 5 shows the dispersion diagram of the TUE structure. As can be observed from Fig. 5, a triple-bandgap is obtained. The bandgaps are defined from different modes that are propagated in the area restricted by the light lines. In there, the first bandgap centered at 7.75 GHz and spans the frequency from 6.67 to 8.83 GHz, which is formed between the first mode and the second mode. Here the first and the second mode are TM and TE mode, respectively. As shown in Fig. 4, the conventional UC-EBG has the bandgap, which is swept from 8.5 – 9.42 GHz with central frequency of 8.96GHz. With the same period of the lattice, the first bandgap of the proposed EBG structure works at a lower frequency than that of conventional UC-EBG. It proves that the proposed EBG structure is more compact in size.

Two remainder bandgaps are determined by the higher TE modes. The second bandgap spans from 9.9 to 10.99 GHz with central frequency of 10.445 GHz. Finally, it is observed that the third bandgap is centered at 13.005 GHz with a bandwidth spreading from 11.97 predicted to 14.04 GHz. The third central frequency f_{C3} can be predicted from the equation (5). Table 2 represents the relative central frequency f_{C3} corresponding to different value of b in case of prediction and simulation. As can be shown in Table 2, the prediction results agree well with the one of the simulation as b = 2 mm. The deviation in this situation is only 1.1%. The more b increases the more deviation increase. However, this method is relative available for predicting the third bandgap in a range of frequencies.

Table 1: Design specifications for each EBG unit cell.

BG type	**Design parameters (mm)**						
CUE	**a**	**g**	**c**	**s**	**l**	**b**	
	7.2	0.6	3	1	2	2	
TUE	**a**	**g**	**c**	**s**	**l**	**b**	**k**
	7.2	0.6	3	1	2	2	0.25
	i	**w**	**u**	**p**	**c**	**e**	**d**
	0.2	0.2	0.2	0.2	0.2	0.2	0.2

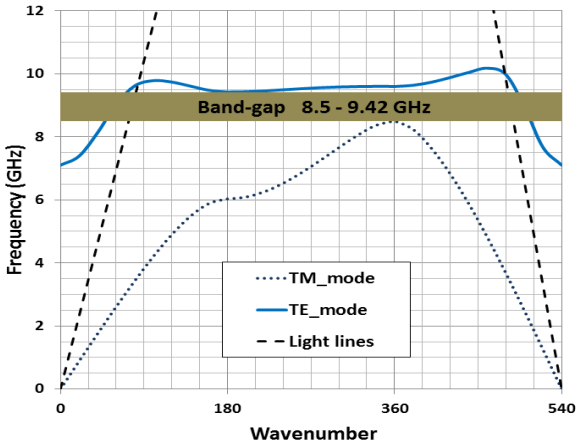

Figure 4: Dispersion diagram of conventional UC-EBG structure

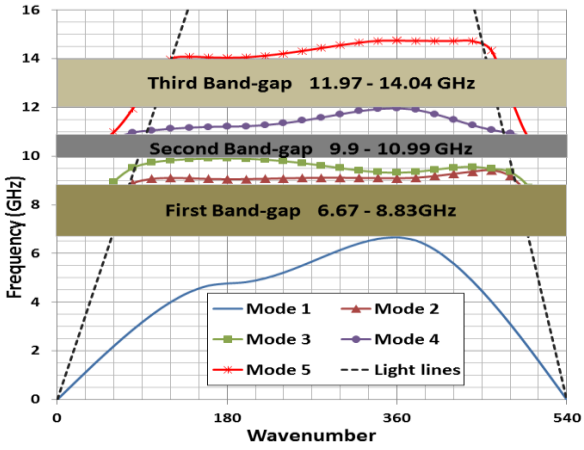

Figure 5: Dispersion diagram of proposed triple-band EBG structure

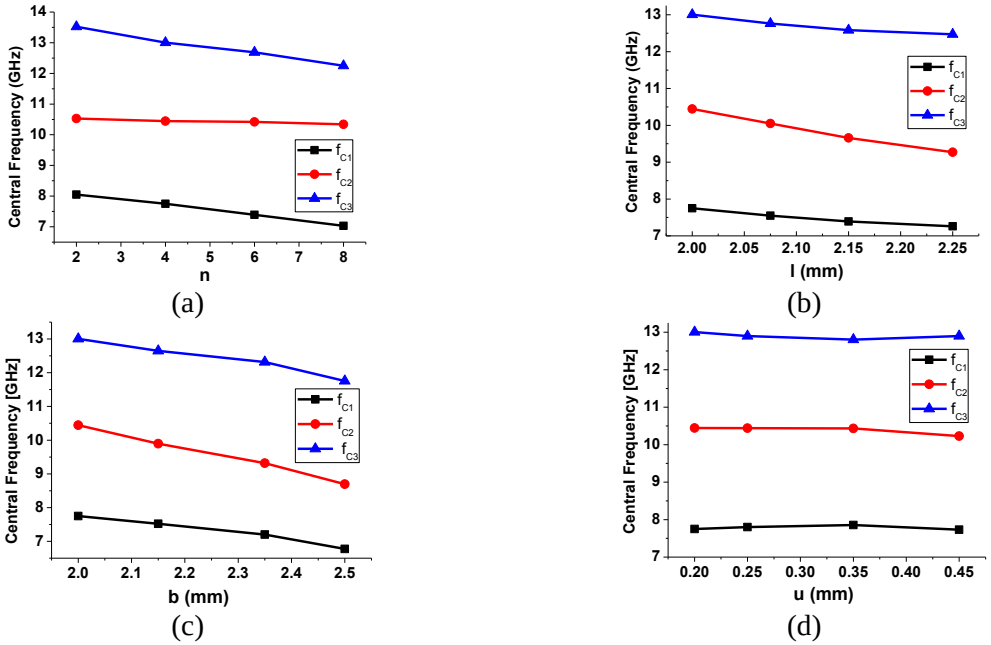

Figure 6: Curve to relate the central frequencies to the value of parameters (when one parameter is changed, the other parameters are fixed). (a) Different value of *n*, (b) Different value of *l*, (c) Different value of *b* and (d) Different value of *u*.

Next, the effect of the parameters of the changing of the central frequencies is investigated. As shown in Fig. 6a, all three resonant frequencies tend to drop down with the increasing of the steps of meandered line, *n*. These can be demonstrated clearly from the equation (3). When *n* increase, the parasitic capacitance C_{Pi} increase then the central frequency f_{C1} inversely decrease. Moreover, the more *l* increases the more the r_{out} and r_{in} increase. As the equation (4a) and (4c), it is shown that when r_{out} and r_{in} increase, the higher capacitance C_{21} and C_{22} are obtained. This leads to the decreasing of the second central frequency f_{C2} as the equation (4d). It is indicated clearly in Fig. 6(b). Learn from Fig. 6(c), the increasing of *b* leads to the decreasing of three central frequencies. As the equation (5b), it is shown that the length of the L-shaped slot increases when the extending of *b* is utilized and then the decreasing of the third central frequency are obtained as the equation (5).

As can be observed from the Fig. 6(d), three central frequencies are almost not varying. This can be explained as follows: the increasing of *u* leads to the increasing of C_{23} as equation 4(b) and 4(c). Besides, the radius of the inner circumcircle r_{in} is decreased when *u* increase. Therefore, the lower capacitance C_{21} and C_{22} are resulted in the equation (4a) and (4c). It is clear that C_{21} and C_{22} are

inversely proportional to C_{23} in this situation. Thus, the second central frequency f_{C2} is almost not changing as the equation (4e).

Table 3 describes the relative reduction of three central frequencies for different parameters when one parameter is changed, and the other parameters are fixed. It is found that the reduction of first central frequency is highest at 9.3% when the steps of meander line *(n)* increase by two times. The second central frequency is the most reduction frequency that is obtained at 11.25% and 16.75% corresponding to the size increasing of *l* and *b* at 12.5% and 25%, respectively.

Table 2: Relative third central frequency of proposed EBG structure for various *b*

Value of *b* (mm)	Third central frequency f_{C3}		Deviation (%)
	Predicted (GHz)	Simulated (GHz)	
2	12.86	13.005	1.1
2.15	11.85	12.65	6.3
2.35	10.74	12.315	12.7
2.5	10	11.755	14.9

Table 3: Relative of the central frequency reduction for different parameters of triple-band EBG structure

Parameter	Increment of parameter	Central frequency reduction (%)		
		Fist Bandgap	Second Bandgap	Third Bandgap
n	2 (times)	9.3	1	5.8
l	12.5 (%)	6.3	11.25	4.1
b	25 (%)	12.6	16.75	9.6

By adjusting one of the parameters of the proposed EBG structure, the central frequency of bandgap can be varied over a frequency range. Moreover, the central frequencies are more reduced by increasing multi parameter at the same time. Table 4 illustrates the effect of the adjusting of multi parameter to the reduction of three central frequencies.

The situation A is defined with $n = 4$ and $l = 2$ mm. The situation B is defined with only *n* increases from 4 to 6 while *l* was kept constant at 2 mm. The last case C investigates the variety of *l* with $n = 6$. As shown in Table 4, the reduction of three central frequencies in the case C is higher than the one of the situation B. When the length of the edge conductor increases by 15% then these deviations are obtained at 12.4%, 12.5% and 7.58% in the first, the second and the third central frequency, respectively. This tunable feature should make the proposed EBG structure useful in practical application. One EBG structure can be used in a series of bandgaps without changing the periodic length.

To further validate the properties of the TUE structure, an experiment concerning transmission through the above TUE has been carried out [17]. A 4×5 lattice of the TUE is mounted on a grounded dielectric slab and connected with 50Ω microstrip lines at both ends as the filter structure. This schematic was simulated and takes into comparison with the measurement of the fabrication. The measured results using Anritsu 37369D vector network analyzer are the S21parameter of the proposed structure. The top view and measurement setup of the structure are shown in Fig. 7. The bandgap bandwidth defined with S21 is below -20 dB. The simulation and the measurement of transmission coefficient S21 are shown in Fig. 8.

Table 4: Relative of the central frequency reduction for the variation of multi parameters at the same time

l (mm)	f_{C1} (GHz)			f_{C2} (GHz)			f_{C3} (GHz)		
	A	B	C	A	B	C	A	B	C
2.1	7.75	7.39	7.06	10.445	10.42	9.78	13.005	12.69	12.35
2.2			6.75			9.32			12.03
2.3			6.42			8.89			11.69

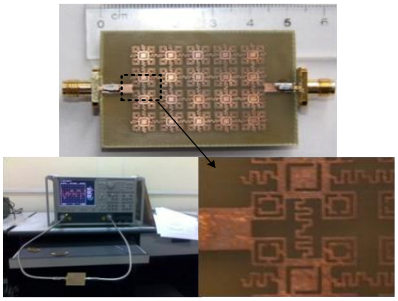

Figure 7: Photo of a 4×5 proposed EBG array and measurement setup.

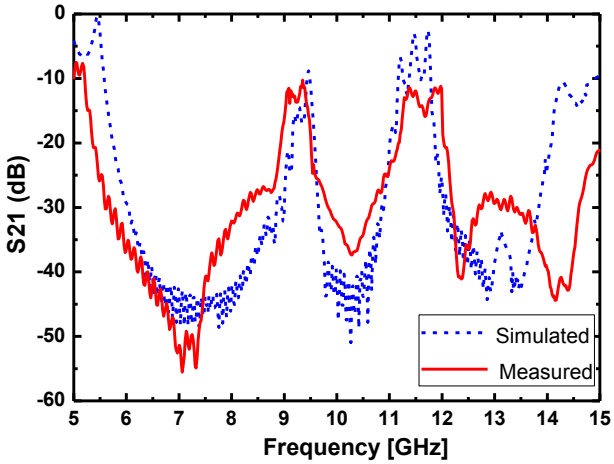

Figure 8: Simulated and measured result of a 4×5 proposed EBG array.

Table 5: Central frequency of triple-band EBG structure

Results of methods	Central frequency (GHz)		
	Fist Bandgap	Second Bandgap	Third Bandgap
Dispersion Diagram	7.750	10.445	13.005
S21 simulated	7.680	10.365	12.883
S21 measured	7.593	10.385	13.520

As can be observed from Fig. 8, the central frequencies of three bandgap of the S21 simulation are good agreement in comparison to the dispersion analysis results. The S21 measurement results are also similar as two results above in the first and the second bandgap. However, there was a large deviation from the third bandgap. The causes that lead to the discrepancies are probably due to few reasons as follows: (1) the error of simulation; (2) the error of the substrate material and (3) the error of fabrication. The first reason may have a little influence on the measurement. However, it is not the main reason because the simulation of transmission coefficient and dispersion diagram is similar. Therefore, the error of the substrate parameters is a possible reason. As [18], it has been demonstrated that the cause of these differences is clearly the error of the unstable FR4 parameters. Besides, the error due to the fabrication is also a major reason. The detailed results are summarized in Table 5.

IV. CONCLUSION AND FUTURE WORK

A novel compact triple-band UC-EBG structure has been presented in this paper. The band-stop properties of the structure have been investigated by using the in-house developed computational tool based on the FDTD method. Simulations and experiments have been performed. The triple-bandgap obtain include the frequency bands at 5.35 – 8.87 GHz, 9.52 – 11.18 GHz and 12.05 - 14.04 GHz, respectively. The measured results are agreeing well with the simulated results. It has been demonstrated that the complete triple-bandgap can be obtained by simply distorting the conventional UC-EBG. Moreover, the central frequencies of three bandgaps can easily vary in a

range of frequency by adjusting one or multi parameters that are not changing the periodic spacing of cell.

In future study it is planned to use the proposed EBG design as high impedance ground plane. A multi-band antenna for WLAN and WiMAX systems will be designed. The bandgaps of the proposed EBG structure will be controlled to meet the frequency bands of these systems. Then the EBG structure will be integrated with the multi-band antennas for reducing back radiation and increasing radiation efficiency of the antenna.

REFERENCES

[1]. E. Rajo-Iglesias, L. Inclan-Sanchez, J. L. Vazquez-Roy, and E. Garcia-Muoz, (2007) "Size reduction of mushroom-type EBG surfaces by using edge- located vias," *IEEE Microw. Wireless Compon. Lett.*, Vol. 17, No. 9, pp 670–672.

[2]. F. Yang and Y. Rahmat-Samii, (2003) "Microstrip antennas integrated with electromagnetic bandgap (EBG) structures: A low mutual coupling design for array applications," *IEEE Trans. Antenna Propag.*, Vol. 51, No. 10, pp 2936–2946.

[3]. O. Folayan and R. Langley, (2009) "Dual frequency band antenna combined with a high impedance band gap surface," *IET Microwaves, Antennas Propag.*, Vol. 3, No. 7, pp 1118–1126.

[4]. G. Goussetis, A. P. Feresidis, and J. C. Vardaxoglou, (2006) "Tailoring the AMC and EBG characteristics of periodic metallic arrays printed on grounded dielectric substrate," *IEEE Trans. Antennas Propag.*, Vol. 54, No. 1, pp 82–89.

[5]. C. Cheype, C. Serier, M. Thevenot, T. Monediere, A. Reineix, and B. Jecko, (2002) "An electromagnetic bandgap resonator antenna," *IEEE Trans. Antennas Propag*., Vol. 50, No. 9, pp 1285–1290.

[6]. D. Sievenpiper, L.J. Zhang, R. F. J. Broas, N. G. Alexopolous, and E. Yablonovitch, (1999) "High-impedance electromagnetic surface with a forbidden frequency band," *IEEE Trans. Microw. Theory Tech.*, Vol. 47, No. 11, pp 2059-2074.

[7]. L. Yang, M. Fan, F. Chen, J. She, and Z. Feng, (2005) "A Novel Compact Electromagnetic-Bandgap (EBG) Structure and Its Applications for Microwave Circuits," *IEEE Trans. Microw. Theory Tech.*, Vol.53, No. 1, pp 183-190.

[8]. W. Wang, X. Cao, R. Wang, J. Ma, (2008) "A Small Dual-band EBG Structure for Microwave," *International Conference on Microwave and Millimeter wave Technology*.

[9]. L.-J. Zhang, C.-H. Liang, L. Liang, and L. Chen, (2008) "A Novel Design Approach For Dual-Band Electromagnetic Bandgap Structure" *Progress In Electromangetics Research M*, Vol. 4, pp 81–91.

[10]. T. Masri, M.K.A. Rahim, and M.N.A. Karim, (2007) "A Novel 2D Sierpinski Gasket Electromagnetic Bandgap Structure for Multiband Microstrip Antenna," *Proceeding of Asia-Pacific Conference on Applied Electromagnetics*.

[11]. R. Kumar, G. Mathai, and J.P. Shinde, (2009) "Design of Compact Multiband EBG and Effect on Antenna Performance," *International Journal of Recent Trends in Engineering*, Vol. 2, No. 5, pp 254–258.

[12]. L. Peng, C. L. Ruan and Z. Q. Li, (2010) "A Novel Compact and Polarization-Dependent Mushroom-Type EBG Using CSRR for Dual/Triple-Band applications," *IEEE Microw. Wireless Compon. Lett*., Vol. 20, No. 9, pp 489–491.

[13]. Allen Taflove and Susan C. Hagness, (2000) *Computational Electrodynamics: The Finite-Difference Time-Domain Method*, Artech House, 2nd Ed., MA.

[14]. Q. Wu, M. F. Wu, F. Y. Meng, J. W and L. W. Li, (2005) "Modelling the Effects of an Individual SRR by Equivalent Circuit Method," *IEEE AP-S International Symposium and USNC/URSI National Radio Science Meeting*.

[15]. M. F. Wu, F. Y. Meng, and Q. Wu, (2005) "A Compact Equivalent Circuit Model for the SRR Structure in Metamaterials," *Asia-Pacific Microwave Conference*.

[16]. Vidyalakshmi.M.R and Dr.S. Raghavan, (2010) "Comparison of Optimization Techniques for Square Split Ring Resonator," *Intl. J. of Microwave and Optical Tech.,* Vol. 5, No. 5.

[17]. B.Q. Lin, Q.R. Zheng and N.C. Yuan, (2006) "A novel planar PBG structure for size reduction," *IEEE Microw. Wireless Compon. Lett*., Vol. 16, NO. 5, pp 269–271.

[18]. L. Peng and C.L. Ruan, (2011) "UWB Band-Notched Monopole Antenna Design Using Electromagnetic-Bandgap Structures," *IEEE Trans. Antenna Propag.*, Vol. 59, No. 4, pp 1074–1081.

AUTHORS

Huynh Nguyen Bao Phuong received the B.E and M.Sc. degrees in 2003 and 2007, respectively, from School of Electronics and Telecommunications, Hanoi University of Science and Technology, Vietnam. Now he is a Lecturer of the Faculty of Technique and Technology, Quynhon University, Vietnam. Currently, he is working toward the Ph.D degree at the School of Electronics and Communications, Hanoi University of Science and Technology, Vietnam. His research interests are high impedance surfaces (HIS), ultra wideband (UWB), microstrip and metamaterial antennas.

Dao Ngoc Chien received the Diploma of Engineer in 1997 from the Department of Telecommunication Systems, School of Electronics and Telecommunications, Hanoi University of Science and Technology, where in the same year he became a Teaching Assistant. He received M.Sc. and Ph.D. degrees in 2002 and 2005, respectively, from the Department of Electronics and Computer Engineering, Gifu University, Japan. At the Department of Telecommunication Systems, School of Electronics and Telecommunications, Hanoi University of Science and Technology, he worked as the Senior Lecturer from 2005 to 2011, and is currently the Contracted Lecturer. He has been appointed to Associate Professor since November, 2010. His research interests include computational electromagnetics based on MoM and FDTD methods, analysis and design of modern antennas and of nanometric integrated optical circuits based on the surface plasmon polaritons. He has been a reviewer for several journals/transactions of Optical Society of America (OSA), Institute of Electrical and Electronics Engineers (IEEE), Elsevier, and American Geophysical Union (AGU), as well as for a number of conferences. He has been a member of IEEE, OSA and REV.

Tran Minh Tuan (Assoc. Prof. Ph.D) was born in Hanoi – Vietnam in 1970. He received the B.E degree and M.E degree in Satellite Communications from Moscow Institute of Technology in Russia in 1994 and in 1995, respectively. In 2004, he received Ph.D degree in antenna and radiowave propagation in Hanoi University of Science and Technology, Vietnam. Now he is Vice President of National Institute of Information and Communications Strategy, Ministry of Information and Communications of Vietnam. His current research interests includes: master plans and strategies of telecommunications and IT development in Vietnam, radiowave broadcasting and propagation, slow-wave structures, slotted, leaky-wave and microstrip antennas, CAD software for radio-wave structures, slotted, leaky-wave and microstrip antennas etc.